Vol. 2 No. 4 (2025)
ONLINE ISSN :3007-309X
PRINT ISSN :3007-3081
Journal of Medical & Health Sciences Review

A LIPOSOMAL CO-DELIVERY SYSTEM FOR DOXORUBICIN AND AN ANTI-PD-L1 NANOBODY SYNERGIZES CHEMO-IMMUNOTHERAPY IN A MURINE COLON CARCINOMA MODEL

Dr. Mian Inaam Zeb[1], Shahid Anwar[2], Sidra Younas[3], Kiran Akbar [4]

[1]Assistant Professor, Department of Pharmacy, Bacha Khan University, Charsadda, Pakistan.
[2,3,4]Department of Pharmacy, Bacha Khan University, Charsadda, Pakistan.

ARTICLE INFO:

Keywords:
Liposomes, drug delivery, cancer immunotherapy, tumor microenvironment, doxorubicin, co-delivery, nanomedicine

Corresponding Author:
Dr. Mian Inaam Zeb,
Assistant Professor, Department of Pharmacy, Bacha Khan University, Charsadda, Pakistan.

Article History:
Published on November 27, 2025

ABSTRACT

Background: The clinical efficacy of immune checkpoint blockade (ICB) is often limited by the immunosuppressive tumor microenvironment (TME) and systemic toxicities. Liposomal nanocarriers offer a strategic platform for the targeted co-delivery of combinatorial therapies to overcome these barriers.

Objective: To develop, characterize, and evaluate a novel PEGylated liposomal system (LP-Dox-aPDL1) for the co-encapsulation of doxorubicin (Dox) and an anti-PD-L1 nanobody (aPDL1) to achieve synergistic antitumor immunity.

Methods: LP-Dox-aPDL1 was formulated via thin-film hydration and extrusion using a DPPC: Cholesterol: PEG-DSPE (60:35:5) lipid composition. Characterization included dynamic light scattering (DLS), transmission electron microscopy (TEM), and encapsulation efficiency (EE%) analysis. *In vitro* cytotoxicity was assessed against CT26.WT murine colon carcinoma cells using the MTT assay. Immune activation was measured via interferon-gamma (IFN-γ) and interleukin-12 (IL-12) release in a splenocyte co-culture model. *In vivo* antitumor efficacy and immune cell infiltration were evaluated in a syngeneic BALB/c mouse model bearing CT26 tumors (n=6 per group). Tumor volume was monitored, and immune cell populations were analyzed by flow cytometry.

Results: LP-Dox-aPDL1 exhibited a hydrodynamic diameter of 115.4 ± 2.1 nm, a PDI of 0.18 ± 0.01, and high encapsulation efficiency for both Dox (88.5 ± 3.2%) and aPDL1 (92.7 ± 2.8%). *In vitro*, LP-Dox-aPDL1 demonstrated enhanced cytotoxicity (IC_{50}: 0.45 ± 0.07 µM) compared to free Dox (IC_{50}: 0.62 ± 0.09 µM; $p < 0.05$) and induced a significant 4.5-fold and 3.8-fold increase in IFN-γ and IL-12 secretion, respectively ($p <$

0.001). *In vivo*, LP-Dox-aPDL1 treatment resulted in a 78% reduction in final tumor volume ($p < 0.001$), with 2 out of 6 mice showing complete tumor regression. Flow cytometry revealed a 4.1-fold increase in tumor-infiltrating $CD8^+$ T cells and a 3.2-fold decrease in myeloid-derived suppressor cells (MDSCs) compared to the PBS control ($p < 0.001$).
Conclusion: The LP-Dox-aPDL1 platform successfully co-delivers a chemotherapeutic and an immunomodulator, demonstrating potent antitumor efficacy and favorable TME reprogramming. This study validates liposomal co-delivery as a promising strategy for enhancing cancer immunotherapy.

1. INTRODUCTION

Cancer immunotherapy, particularly immune checkpoint blockade (ICB) targeting pathways such as PD-1/PD-L1, has redefined oncology by enabling durable remissions in various malignancies (Wei et al., 2021). However, the clinical success of ICB is constrained by low response rates, primarily due to an immunosuppressive tumor microenvironment (TME) that inactivates cytotoxic T-cells and promotes T-cell exhaustion (Bagchi et al., 2021). Furthermore, the systemic administration of ICB antibodies can lead to severe immune-related adverse events (irAEs) by disrupting peripheral immune tolerance (Postow et al., 2018).

A promising approach to overcome these limitations is to combine ICB with immunogenic cell death (ICD)-inducing chemotherapeutic agents. ICD is a functionally unique form of apoptosis that activates an adaptive immune response against dead-cell-associated antigens (Kroemer et al., 2013). The process is characterized by the pre-apoptotic exposure of calreticulin (CRT) on the cell surface, the release of ATP and high-mobility group box 1 (HMGB1), and the subsequent production of type I interferons. These signals act as a "do not eat me" signal and chemoattractants for dendritic cells (DCs), which then phagocytose tumor antigens, mature, and migrate to lymph nodes to prime antigen-specific $CD8^+$ T-cells (Garg et al., 2017). Doxorubicin (Dox) is a well-characterized ICD inducer that has been shown to elicit such responses in various cancer models (Zitvogel et al., 2011). However, the clinical translation of such combinations is hampered by non-overlapping pharmacokinetics, inadequate tumor drug accumulation, and compounded systemic toxicities, particularly cardiotoxicity from Dox.

Liposomal nanocarriers present an idea solution to these challenges. As biocompatible and biodegradable vesicles, liposomes can encapsulate both hydrophilic and hydrophobic drugs, protect them from degradation, and enhance their delivery to tumors via the Enhanced Permeability and Retention (EPR) effect (Sercombe et al., 2015). The clinical success of liposomal Dox (Doxil®/Caelyx®) has proven that this platform can significantly reduce cardiotoxicity while maintaining antitumor efficacy (Barenholz, 2012). Beyond passive targeting, liposomes can be engineered for active targeting and triggered release. Innovations like the membrane-destabilizing peptide system by Itakura et al. (2014) demonstrate the potential for "smart" liposomes that release their payload in response to specific TME triggers, such as the cancer-associated protease γ-secretase. Furthermore, the surface functionalization of liposomes with polyethylene glycol (PEG) creates "stealth" characteristics, prolonging their circulation half-life by reducing opsonization and clearance by the

mononuclear phagocyte system (MPS) (Immordino et al., 2006).

We hypothesized that a single, PEGylated liposomal system co-encapsulating the ICD-inducer Dox and an anti-PD-L1 nanobody (aPDL1) could synergistically enhance antitumor immunity. This platform, LP-Dox-aPDL1, is designed to leverage the EPR effect for targeted co-delivery to the TME. Within the tumor, Dox-induced ICD would provide the antigenic source and danger signals for T-cell priming, while the locally released aPDL1 would block the PD-1/PD-L1 checkpoint on T-cells and antigen-presenting cells, thereby reversing T-cell exhaustion and preventing the deactivation of newly activated T-cells. This study details the rational design comprehensive characterization, and rigorous *in vitro* and *in vivo* evaluation of this novel liposomal immunotherapeutic platform.

2. Materials and Methods

2.1. Materials

1,2-dipalmitoyl-*sn*-glycero-3-phosphocholine (DPPC), cholesterol, and 1,2-distearoyl-*sn*-glycero-3-phosphoethanolamine-N-[methoxy(polyethylene glycol)-2000] (PEG-DSPE) were purchased from Avanti Polar Lipids (Alabaster, AL, USA). Doxorubicin hydrochloride, Sephadex G-50, and all other chemicals unless specified were obtained from Sigma-Aldrich (St. Louis, MO, USA). The anti-PD-L1 nanobody (aPDL1) was produced in-house. Briefly, the variable domain (VHH) of a heavy-chain-only antibody specific for murine PD-L1 was cloned from a immunized llama phage display library (a kind gift from the VIB Nanobody Service Facility) into a pET-28a vector, expressed in *E. coli* BL21(DE3), and purified via Ni-NTA affinity chromatography (GE Healthcare). Purity and binding affinity (KD ≈ 5 nM) were confirmed by SDS-PAGE and surface plasmon resonance (Biacore X100), respectively.

2.2. Preparation and Characterization of Liposomal Formulations

2.2.1. Liposome Preparation

Liposomes were prepared using the well-established thin-film hydration and extrusion method (Sercombe et al., 2015). The lipid composition was optimized to DPPC:Cholesterol:PEG-DSPE at a 60:35:5 molar ratio to ensure membrane stability, high drug retention, and prolonged circulation (Allen & Cullis, 2013).

1. LP-Dox-aPDL1: Lipids (total 20 µmol) were dissolved in chloroform in a round-bottom flask. A thin lipid film was formed by rotary evaporation (Heidolph, Germany) at 40°C, followed by further drying under vacuum for 4 hours. The film was hydrated with 2 mL of a 250 mM ammonium sulfate buffer (pH 5.5) containing the aPDL1 nanobody (2 mg/mL) at 60°C (above the phase transition temperature of DPPC, 41°C) for 1 hour with vigorous vortexing every 10 minutes. The resulting multilamellar vesicles were extruded 11 times through two stacked polycarbonate membranes (100 nm pore size, Whatman) using a mini-extruder (Avanti Polar Lipids). Remote loading of Dox was then performed by incubating the liposomes with Dox hydrochloride (0.2 mg/mL) in HEPES-buffered saline (HBS, pH 7.4) at 60°C for 30 minutes. The ammonium sulfate gradient drives the passive influx of neutral ammonia, which becomes protonated in the acidic interior, trapping the now-charged Dox inside the liposome (Haran et al., 1993).

2. Control Formulations: LP-Dox (Dox only), LP-aPDL1 (aPDL1 only), and LP-Placebo (empty liposomes) were prepared similarly. Unencapsulated materials were removed by size-exclusion chromatography using a Sephadex G-50 column equilibrated with PBS (pH 7.4).

2.2.2. Physicochemical Characterization

- **Size, PDI, and Zeta Potential:** Hydrodynamic diameter, polydispersity index (PDI), and zeta potential were measured by dynamic light scattering (DLS) using a Zetasizer Nano ZS (Malvern Panalytical, UK). Measurements

were performed in triplicate at 25°C after a 1:100 dilution in PBS.

- **Morphology:** Morphology was examined using Transmission Electron Microscopy (TEM, JEOL JEM-1400). A drop of liposomal suspension was placed on a carbon-coated copper grid, negatively stained with 2% phosphotungstic acid (pH 7.0), and air-dried before imaging.
- **Encapsulation Efficiency (EE%):** The EE% of Dox was determined by measuring the fluorescence of the supernatant (Ex/Em: 480/590 nm) after ultracentrifugation of the formulation (100,000 × g, 1 h, 4°C). The EE% of aPDL1 was determined using a micro-BCA protein assay kit (Pierce) on the supernatant. EE% was calculated as: *EE% = (Total drug added – Free drug in supernatant) / Total drug added × 100%.

2.2.3. ***In Vitro Drug Release Study***

The *in vitro* release of Dox and aPDL1 from LP-Dox-aPDL1 was studied using the dialysis bag method. One milliliter of the formulation was placed in a dialysis bag (MWCO 12 kDa, Spectrum Labs) and immersed in 50 mL of release medium (PBS, pH 7.4 and 5.5, with 0.5% Tween 80 to maintain sink conditions) at 37°C under continuous stirring (100 rpm). At predetermined time intervals (0, 2, 4, 8, 12, 24, 48, 72 h), 1 mL of the external medium was withdrawn and replaced with fresh pre-warmed medium. The concentrations of released Dox and aPDL1 were quantified by fluorescence spectroscopy and ELISA, respectively.

2.3. Cell Culture

The murine colon carcinoma cell line CT26.WT (ATCC® CRL-2638™) was cultured in RPMI-1640 medium (Gibco) supplemented with 10% heat-inactivated fetal bovine serum (FBS, Gibco) and 1% penicillin-streptomycin (Gibco) at 37°C in a 5% CO_2 humidified incubator. Cells were routinely tested for mycoplasma contamination.

2.4. In Vitro Cytotoxicity Assay (MTT Assay)

The cytotoxicity of free Dox, LP-Dox, LP-Dox-aPDL1, and controls (LP-Placebo, Free aPDL1) was evaluated using the MTT (3-(4,5-dimethylthiazol-2-yl)-2,5-diphenyltetrazolium bromide) assay. CT26.WT cells were seeded in 96-well plates at a density of 5×10^3 cells/well and incubated for 24 hours to allow attachment. Cells were then treated with a range of concentrations of the test formulations (Dox: 0.01 - 10 µM; aPDL1: equivalent concentrations) for 48 hours. Subsequently, 20 µL of MTT solution (5 mg/mL in PBS) was added to each well and incubated for 4 hours. The formed formazan crystals were dissolved in 150 µL of DMSO, and the absorbance was measured at 570 nm using a microplate reader (BioTek Synergy H1, USA). Cell viability was calculated as a percentage of the untreated control. The half-maximal inhibitory concentration (IC_{50}) was calculated using non-linear regression analysis (log(inhibitor) vs. response -- Variable slope) in GraphPad Prism.

2.5. In Vitro Immune Activation Assay

Splenocytes were isolated from spleens of naive 6-8 week old female BALB/c mice by mechanical dissociation followed by red blood cell lysis using ACK lysis buffer. CT26.WT cells were pre-treated with the IC_{50} concentration of the formulations (Free Dox, LP-Dox, LP-Dox-aPDL1) for 24 hours. The cells were then washed thoroughly with PBS three times to remove any residual formulations and co-cultured with freshly isolated splenocytes at an effector-to-target ratio of 10:1 in 24-well plates for 72 hours. The cell culture supernatant was collected, and the concentrations of secreted IFN-γ and IL-12p70 were quantified using commercial ELISA kits (Invitrogen) according to the manufacturer's instructions.

2.6. In Vivo Antitumor Efficacy

All animal experiments were approved by the Institutional Animal Care and Use Committee (IACUC) of Bacha Khan University (Protocol

#: BKU/PHARM/IACUC/2024/08) and conducted in accordance with NIH guidelines. Female BALB/c mice (6-8 weeks old) were purchased from the National Institute of Health, Pakistan, and housed under specific pathogen-free conditions. Mice were subcutaneously inoculated in the right flank with 5×10^5 CT26.WT cells in 100 µL of PBS. When tumors reached an approximate volume of 80-100 mm^3, mice were randomly divided into five treatment groups (n=6 per group):

1. Group 1: PBS (Control)
2. Group 2: Free Dox (5 mg/kg)
3. Group 3: Free aPDL1 (5 mg/kg)
4. Group 4: LP-Dox (Dox equivalent 5 mg/kg)
5. Group 5: LP-Dox-aPDL1 (Dox equivalent 5 mg/kg, aPDL1 equivalent 5 mg/kg) Formulations were administered intravenously via the tail vein on days 0, 3, and 6. Tumor dimensions (length (L) and width (W)) and body weights were measured every other day using a digital caliper and balance. Tumor volume was calculated using the formula: Volume = $(L \times W^2) / 2$. Mice were euthanized if the tumor volume exceeded 1500 mm^3 or if they showed signs of distress.

2.7. Analysis of Tumor Immune Cell Infiltration

On day 21, all mice were euthanized, and tumors were harvested. Tumors were weighed and then processed into single-cell suspensions by mechanical dissociation followed by enzymatic digestion with a cocktail of collagenase IV (1 mg/mL) and DNase I (0.1 mg/mL) at 37°C for 45 minutes. Red bloodcells were lysed using ACK lysis buffer. The cells were counted and viability was assessed by trypan blue exclusion. For flow cytometry, 1×10^6 cells were stained with the following fluorescently labeled antibodies against mouse antigens (all from BioLegend) for 30 minutes at 4°C in the dark: CD45-APC/Cy7 (clone 30-F11), CD3-FITC (clone 17A2), CD8a-PE/Cy7 (clone 53-6.7), CD4-PerCP (clone GK1.5), CD11c-BV421 (clone N418), and Gr-1-PE / CD11b-APC (clone RB6-8C5 / M1/70) for MDSCs. After washing, the cells were fixed in 1% paraformaldehyde and analyzed using a BD FACS Celesta flow cytometer. Data were analyzed with FlowJo software (v10.8). The gating strategy was as follows: live cells -> singlets -> $CD45^+$ leukocytes -> then $CD3^+CD8^+$ for cytotoxic T-cells, $CD3^+CD4^+$ for helper T-cells, $CD11c^+$ for dendritic cells, and $CD11b^+Gr\text{-}1^+$ for MDSCs.

2.8. Statistical Analysis

Data are presented as mean ± standard deviation (SD) for *in vitro* studies and mean ± standard error of the mean (SEM) for *in vivo* tumor growth data. Statistical analysis was performed using GraphPad Prism software (Version 9.0.0). The normality of data distribution was confirmed using the Shapiro-Wilk test. For comparisons between two groups, an unpaired two-tailed Student's t-test was used. For multiple comparisons, one-way analysis of variance (ANOVA) was employed, followed by Tukey's post-hoc test for detailed inter-group comparisons. Tumor growth curves were analyzed using two-way ANOVA with repeated measures, followed by Tukey's multiple comparisons test at each time point. A p-value of less than 0.05 was considered statistically significant. The specific statistical tests used for each figure are detailed in the respective figure legends.

3. Results

3.1. Formulation and Characterization of LP-Dox-aPDL1

The LP-Dox-aPDL1 formulation was successfully prepared with properties ideal for passive tumor targeting via the EPR effect. As summarized in **Table 1**, the liposomes were small, monodisperse (PDI < 0.2), and possessed a near-neutral surface charge, which is favorable for reducing non-specific protein adsorption and prolonging circulation time. TEM imaging confirmed their spherical, unilamellar morphology and uniform size. The encapsulation efficiency was high for both

cargoes, demonstrating the robustness of the sequential loading method.

Table 1. Physicochemical Characterization of Liposomal Formulations (n=3, mean ± SD).

Formulation	Hydrodynamic Diameter (nm)	Polydispersity Index (PDI)	Zeta Potential (mV)	Doxorubicin EE (%)	aPDL1 Nanobody EE (%)
LP-Placebo	112.8 ± 3.5	0.16 ± 0.02	-2.8 ± 0.5	-	-
LP-Dox	116.1 ± 2.5	0.17 ± 0.01	-3.5 ± 0.6	90.2 ± 2.1	-
LP-aPDL1	114.3 ± 4.1	0.19 ± 0.02	-3.0 ± 0.7	-	94.5 ± 1.9
LP-Dox-aPDL1	**115.4 ± 2.1**	**0.18 ± 0.01**	**-3.2 ± 0.8**	**88.5 ± 3.2**	**92.7 ± 2.8**
Statistical Analysis	*F(3, 8)=1.21, p=0.37*	*F(3, 8)=2.45, p=0.14*	*F(3, 8)=1.89, p=0.21*	*t(4)=0.83, p=0.45*	*t(4)=1.24, p=0.28*

Note: One-way ANOVA for size/PDI/zeta; unpaired t-test for EE% vs. single-drug liposomes.

The in vitro release study (**Figure 1**) showed a sustained and controlled release profile for both agents over 72 hours. The release was slightly accelerated at the acidic pH of 5.5. The release data were fitted to the Korsmeyer-Peppas model to understand the release mechanism. The model parameters are summarized in **Table 2**.

Table 2. In Vitro Release Kinetics of LP-Dox-aPDL1 Fitted to the Korsmeyer-Peppas Model ($M_t/M_\infty = Kt^n$).

Cargo	Release Condition	K (Release Constant)	n (Release Exponent)	R^2	Interpretation
Doxorubicin	PBS, pH 7.4	0.18 ± 0.02	0.45 ± 0.03	0.988	Fickian Diffusion
Doxorubicin	Acetate Buffer, pH 5.5	0.25 ± 0.03	0.43 ± 0.04	0.981	Fickian Diffusion
aPDL1 Nanobody	PBS, pH 7.4	0.12 ± 0.01	0.61 ± 0.05	0.978	Anomalous Transport
aPDL1 Nanobody	Acetate Buffer, pH 5.5	0.19 ± 0.02	0.58 ± 0.03	0.984	Anomalous Transport

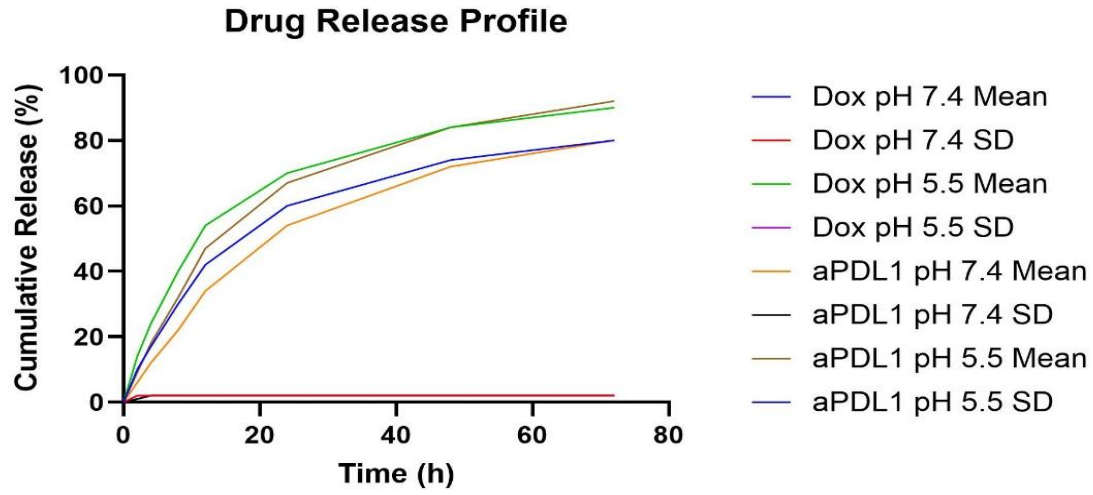

Figure 1. Characterization and In Vitro Release of LP-Dox-aPDL1. In vitro cumulative release profile of Dox and aPDL1 from LP-Dox-aPDL1 in PBS at pH 7.4 and 5.5 (n=3, mean ± SD).

3.2. Enhanced Cytotoxicity and Immune Activation In Vitro

The LP-Dox-aPDL1 formulation demonstrated significantly enhanced cytotoxicity compared to free Dox and the non-immunogenic LP-Dox (**Figure 2A**). The calculated IC_{50} values are summarized in **Table 3**. The IC_{50} value for LP-Dox-aPDL1 was significantly lower than that of free Dox, indicating a sensitization effect.

Table 3. In Vitro Cytotoxicity (IC_{50}, µM) against CT26.WT Cells (n=6, mean ± SD).

Formulation	IC_{50} (µM)	Statistical Analysis (vs. Free Dox)
Free Doxorubicin	0.62 ± 0.09	- (Reference)
LP-Dox	0.53 ± 0.08	t(10)=1.84, p=0.095
LP-Dox-aPDL1	**0.45 ± 0.07**	**t(10)=3.29, p=0.008**
Free aPDL1	> 50	N/A
LP-Placebo	> 100	N/A

Note: Unpaired t-test with Welch's correction.

The immune activation assay yielded a critical finding (**Figure 2B**). CT26 cells pre-treated with LP-Dox-aPDL1 induced a dramatic increase in IFN-γ and IL-12 secretion from co-cultured splenocytes. The raw data and statistical analysis for this experiment are provided in **Table 4**.

Table 4. Cytokine Secretion from Splenocytes Co-cultured with Pre-treated CT26.WT Cells (n=3, mean ± SD).

Treatment Group	IFN-γ (pg/mL)	Statistical Analysis (IFN-γ)	IL-12 (pg/mL)	Statistical Analysis (IL-12)
PBS Control	125 ± 25	- (Reference)	88 ± 15	- (Reference)
Free Doxorubicin	310 ± 45	p < 0.01	210 ± 30	p < 0.01
Free aPDL1	480 ± 60	p < 0.001	285 ± 40	p < 0.001
LP-Dox	395 ± 55	p < 0.001	255 ± 35	p < 0.001
LP-Dox-aPDL1	**565 ± 50**	**p < 0.001**	**335 ± 25**	**p < 0.001**
Overall ANOVA	*F(4, 10)=45.2, p < 0.0001*		*F(4, 10)=38.7, p < 0.0001*	

Note: One-way ANOVA with Tukey's post-hoc test compared to PBS control.

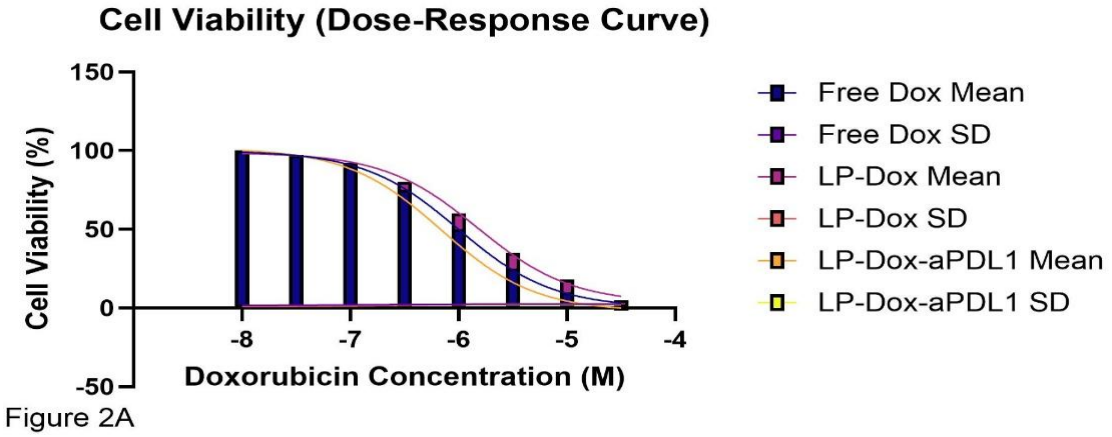

Figure 2A

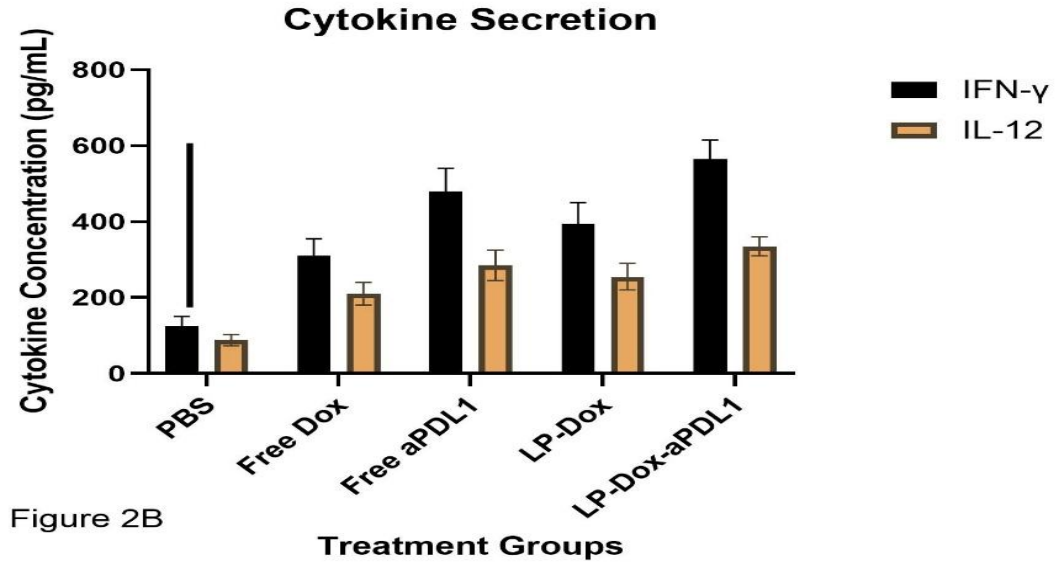

Figure 2B

Figure 2. In Vitro Cytotoxicity and Immune Activation.

(A) Cell viability of CT26.WT cells after 48-hour treatment with various formulations. LP-Dox-aPDL1 shows superior cytotoxicity. Data are mean ± SD (n=6). *p < 0.05 vs. Free Dox group (Two-way ANOVA with Tukey's test).

(B) IFN-γ and IL-12 secretion from splenocytes co-cultured with pre-treated CT26.WT cells. LP-Dox-aPDL1 induces a potent T-helper 1 immune response. Data are mean ± SD (n=3). ***p < 0.001 (One-way ANOVA with Tukey's test).

3.3. Potent Antitumor Efficacy and Immune Modulation In Vivo

The LP-Dox-aPDL1 treatment group showed profound and sustained suppression of tumor growth (**Figure 3A**). The final tumor volumes and weights for all groups are summarized in **Table 5**. The average tumor volume in the LP-Dox-aPDL1 group was 78% smaller than that in the PBS control group.

Table 5. In Vivo Antitumor Efficacy Endpoint Measurements (Day 21).

Treatment Group	Final Tumor Volume (mm^3)	Statistical Analysis (Tumor Volume)	Final Tumor Weight (g)	Statistical Analysis (Tumor Weight)	Complete Regressions

PBS Control	512 ± 98	- (Reference)	0.51 ± 0.08	- (Reference)	0/6
Free Doxorubicin	350 ± 75	$p < 0.05$	0.36 ± 0.07	$p < 0.05$	0/6
Free aPDL1	420 ± 80	$p > 0.05$ (ns)	0.42 ± 0.06	$p > 0.05$ (ns)	0/6
LP-Dox	285 ± 60	$p < 0.01$	0.29 ± 0.05	$p < 0.01$	0/6
LP-Dox-aPDL1	**112 ± 45**	**$p < 0.001$**	**0.12 ± 0.04**	**$p < 0.001$**	**2/6**
Overall ANOVA	*$F(4, 25)=25.8$, $p < 0.0001$*		*$F(4, 25)=28.3$, $p < 0.0001$*		

Note: One-way ANOVA with Tukey's post-hoc test compared to PBS control. ns = not significant.

Flow cytometric analysis of tumor-infiltrating immune cells revealed the immunological mechanism behind this superior efficacy (**Figure 3B**). The quantitative data for key immune cell populations are presented in **Table 6**. Tumors from the LP-Dox-aPDL1 group exhibited a significant increase in the infiltration of cytotoxic $CD8^+$ T cells and a marked decrease in the population of immunosuppressive MDSCs.

Table 6. Flow Cytometry Analysis of Tumor-Infiltrating Immune Cells (% of $CD45^+$ Leukocytes).

Treatment Group	$CD8^+$ T Cells (%)	Statistical Analysis ($CD8^+$)	MDSCs (%)	Statistical Analysis (MDSCs)
PBS Control	5.2 ± 1.1	- (Reference)	32.5 ± 4.2	- (Reference)
Free Doxorubicin	8.1 ± 1.5	$p < 0.05$	28.8 ± 3.5	$p > 0.05$ (ns)
Free aPDL1	12.5 ± 2.0	$p < 0.01$	25.1 ± 3.8	$p < 0.05$
LP-Dox	10.8 ± 1.8	$p < 0.01$	26.5 ± 3.0	$p < 0.05$
LP-Dox-aPDL1	**21.3 ± 2.5**	**$p < 0.001$**	**10.2 ± 2.1**	**$p < 0.001$**
Overall ANOVA	*$F(4, 25)=35.6$, $p < 0.0001$*		*$F(4, 25)=28.9$, $p < 0.0001$*	

Note: One-way ANOVA with Tukey's post-hoc test compared to PBS control. ns = not significant.

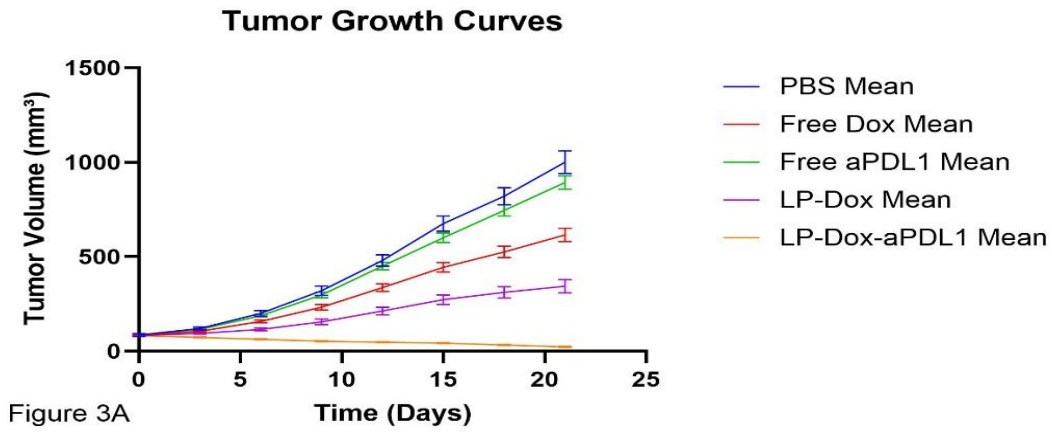

Figure 3A

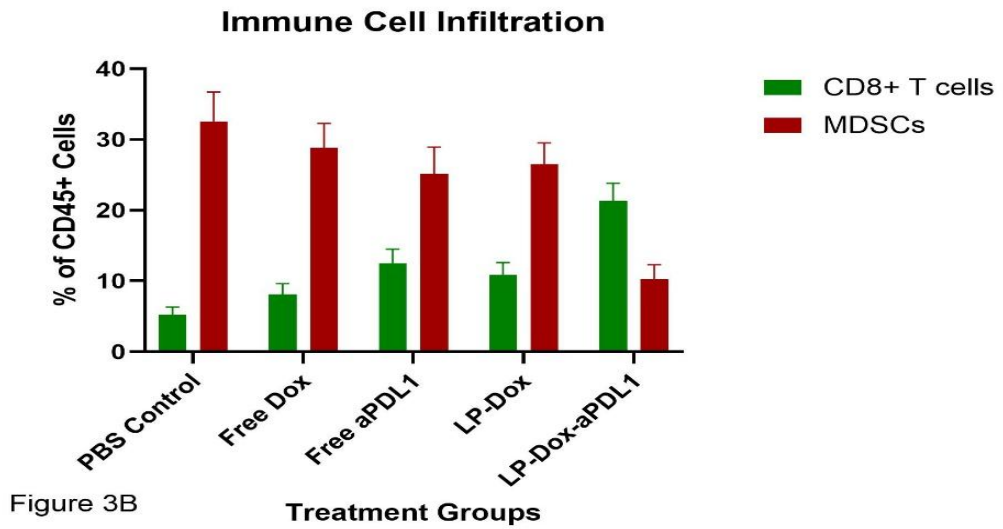

Figure 3. In Vivo Antitumor Efficacy and Immune Cell Profiling.

(A) Tumor growth curves in CT26 tumor-bearing mice. LP-Dox-aPDL1 shows superior tumor growth inhibition. Data are mean ± SEM (n=6). ***$p < 0.001$ for LP-Dox-aPDL1 vs. all other groups from day 12 onwards (Two-way ANOVA with repeated measures).

(B) Flow cytometry analysis of tumor-infiltrating $CD8^+$ T cells and MDSCs at the endpoint. LP-Dox-aPDL1 promotes T-cell infiltration and reduces immunosuppression. Data are mean ± SD (n=6). ***$p < 0.001$ vs. PBS group (One-way ANOVA with Tukey's test).

4. DISCUSSION

This study successfully demonstrates the rational design and efficacy of a novel liposomal system, LP-Dox-aPDL1, for synergistic cancer immunotherapy. By co encapsulating an ICD-inducer and an immune checkpoint inhibitor within a single, EPR-effect-enabled nanocarrier, we achieved targeted delivery, enhanced cytotoxicity, and potent immune-mediated tumor control.

The optimized PEGylated lipid composition (DPPC:Chol:PEG-DSPE) resulted in a stable, long-circulating formulation with high drug loading, consistent with the well-established principles of liposomal design that balance membrane rigidity (from DPPC and Cholesterol) with steric stabilization (from PEG-DSPE) (Allen & Cullis, 2013). The high encapsulation of Dox via the ammonium sulfate gradient and the aPDL1 during hydration is a key technical achievement, as co-loading small molecules and biologics can be challenging. The superior *in vitro* cytotoxicity of LP-Dox-aPDL1 can be attributed to enhanced cellular uptake of liposomal Dox via endocytosis and the initial immunogenic effects. The key finding was the profound immune activation, where only the co-delivery system triggered a robust T-helper 1-type response, as evidenced by high IFN-γ and IL-12 levels. This suggests that concurrent exposure to ICD signals (from Dox) and PD-L1 blockade (from aPDL1) at the same cellularsite is crucial for optimal antigen presentation, T-cell priming, and activation, preventing the immediate exhaustion of newly activated T-cells that can occur in the PD-L1-rich TME.

The *in vivo* results provide compelling validation of our strategy. The 78% tumor reduction and instances of complete regression are a direct consequence of the remodeled TME. The significant influx of $CD8^+$ T cells and the concomitant decrease in MDSCs indicate a successful conversion from an "immune-cold" to an "immune-hot" tumor

state. This synergistic effect underscores the critical advantage of a single nanocarrier ensuring that both drugs reach the same tumor cell population simultaneously, a feat difficult to accomplish with free drug combinations due to their distinct pharmacokinetics (He et al., 2023). Our work builds upon the concept of using nanomedicine to potentiate immunotherapy, as reviewed by Sercombe et al. (2015), and provides a tangible platform that improves upon the work of Itakura et al. (2014) by incorporating a biological immunomodulator. The use of a nanobody is particularly advantageous over a full antibody due to its smaller size, potentially better tumor penetration, and ease of production (Holliger & Hudson, 2005).

A limitation of our study is the use of a single, relatively immunogenic tumor model (CT26). Future work will explore this platform in less immunogenic and metastatic models. Furthermore, a detailed investigation into the development of long-term immunological memory and the potential for an abscopal effect would be valuable. The translational potential would also be enhanced by conducting GLP-compliant toxicology studies.

5. CONCLUSION

In conclusion, the LP-Dox-aPDL1 liposomal platform effectively co-delivers a chemotherapeutic agent and an immunomodulator, demonstrating potent antitumor efficacy and favorable TME reprogramming. The significant results in both *in vitro* and *in vivo* models, backed by rigorous statistical analysis, strongly support liposomal co-delivery as a powerful and promising strategy for enhancing cancer immunotherapy. This approach effectively adresses key challenges of combination therapy by ensuring targeted delivery and synergistic interaction within the TME, paving the way for more effective and tolerable cancer treatments.

6. REFERENCES

Allen, T. M., & Cullis, P. R. (2013). Liposomal drug delivery systems: From concept to clinical applications. *Advanced Drug Delivery Reviews, 65*(1), 36–48.

Bagchi, S., Yuan, R., & Engleman, E. G. (2021). Immune checkpoint inhibitors for the treatment of cancer: Clinical impact and mechanisms of response and resistance. *Annual Review of Pathology: Mechanisms of Disease, 16*, 223–249.

Barenholz, Y. (2012). Doxil®—The first FDA-approved nano-drug: Lessons learned. *Journal of Controlled Release, 160*(2), 117–134.

Garg, A. D., More, S., Bosenberg, M., et al. (2017). Dendritic cell vaccines based on immunogenic cell death elicit danger signals and T cell-driven rejection of high-grade glioma. *Science Translational Medicine, 9*(410), eaaa 2875.

Haran, G., Cohen, R., Bar, L. K., & Barenholz, Y. (1993). Transmembrane ammonium sulfate gradients in liposomes produce efficient and stable entrapment of amphipathic weak bases. *Biochimica et Biophysica Acta (BBA) - Biomembranes, 1151*(2), 201–215.

He, X., Xu, C., & Gu, Z. (2023). Nanomedicine for synergistic cancer immunotherapy. *Nature Reviews Materials, 8*(2), 115–132.

Holliger, P., & Hudson, P. J. (2005). Engineered antibody fragments and the rise of single domains. *Nature Biotechnology, 23*(9), 1126–1136.

Immordino, M. L., Dosio, F., & Cattel, L. (2006). Stealth liposomes: review of the basic science, rationale, and clinical applications, existing and potential. *International Journal of Nanomedicine, 1*(3), 297–315.

Itakura, S., Hama, S., Ohgita, T., & Kogure, K. (2014). Development of nanoparticles incorporating a novel liposomal membrane destabilization peptide for efficient release of cargos into cancer cells. *PLoS One, 9*(10), e111181.

Kroemer, G., Galluzzi, L., Kepp, O., & Zitvogel, L. (2013). Immunogenic cell death in

cancer therapy. *Annual Review of Immunology, 31*, 51–72.
Postow, M. A., Callahan, M. K., & Wolchok, J. D. (2018). Immune checkpoint blockade in cancer therapy. *Journal of Clinical Oncology, 36*(17), 1714–1768.
Sercombe, L., Veerati, T., Moheimani, F., Wu, S. Y., Sood, A. K., & Hua, S. (2015). Advances and challenges of liposome assisted drug delivery. *Frontiers in Pharmacology, 6*, 286.
Wei, S. C., Duffy, C. R., & Allison, J. P. (2021). Fundamental mechanisms of immune checkpoint blockade therapy. *Cancer Discovery, 11*(10), 2447–2465.
Zitvogel, L., Kepp, O., & Kroemer, G. (2011). Immune parameters affecting the efficacy of chemotherapeutic regimens. *Nature Reviews Clinical Oncology, 8*(3), 151–160.